

## Fiber Optic Sensing for Ultrasonic NDE

T. D. Dudderar,<sup>1</sup> C. P. Burger,<sup>2</sup> J. A. Gilbert,<sup>3</sup> J. A. Smith,<sup>2</sup> and B. R. Peters<sup>3</sup>

*Received January 15, 1988; revised April 21, 1988*

An innovative approach to nondestructive evaluation (NDE) using noncontacting optical sensors has demonstrated. In this effort a single mode optical fiber interferometer (OFI) was used to sense the presence and form of Rayleigh waves traveling along the surface of a steel test bar at a velocity of nearly 3mm/ $\mu$ s. Acousto-optic time-domain data was successfully used to detect the presence and locate the position of a test "flaw" (a machined slot) in the bar, and spectrum analysis was used to estimate its geometry and size. This approach has many potential applications in the ultrasonic evaluation of real flaws in structures with complex geometries. Coupled with the authors' earlier work demonstrating the feasibility of generating acoustic waves in metals using laser light pulses transmitted through the fiber optic probes, this latest achievement points to the development of a fully noncontacting, fiber optic based thermal-acousto-photonic (TAP) NDE system, with potential applications to the reliability testing of many important structures where composition, scale, geometry, or restricted access preclude the use of conventional NDE techniques.

**KEY WORDS:** Ultrasonics; fiber optics; lasers.

### 1. INTRODUCTION

The present research effort on thermal-acousto-photonic (TAP) nondestructive evaluation explores the synthesis of conventional ultrasonic excitation/interrogation concepts and sophisticated fiber optic systems with the capacity to inspect, detect, and characterize flaws in a variety of complex and/or inaccessible structures. Since TAP inspection employs photonic sensing, it does not require mechanical coupling of the sensing transducers to the surface of the test structure at the point of detection—a significant advantage over traditional piezoelectric surface contact transducer-based ultrasonic techniques that can be difficult to apply to structures

with complex surface geometries. Since the optical fiber components themselves have low mass, volume, and stiffness, they can be adapted for rapid and automated manipulation, positioning, and scanning. Furthermore, with the laser output confined to optical fibers, operational TAP detection systems can readily be designed in ways that pose little or no occupational health hazard to the operator. In this report it will be shown that, since they are noncontacting (no mass attached to the test surface) point detectors (high spatial resolution), TAP fiber optic sensors can accurately measure an ultrasonic (displacement) response without incurring any deleterious interactions with the interrogating wavefronts. This accuracy assures highly reliable measurement of the propagation characteristics of both transmitted and reflected acoustic waves, greatly facilitating meaningful signal analysis in both the time and frequency domains.

<sup>1</sup>AT&T Bell Laboratories, Murray Hill, New Jersey 07974.

<sup>2</sup>Texas A&M University, College Station, Texas 77843.

<sup>3</sup>University of Alabama-Huntsville, Huntsville, Alabama 35899.

## 2. INTERFEROMETRY

A basic interferometer consists of two coherent beams of light: an object beam, which passes through, or is reflected by, the specimen under observation, and a reference beam, which is unaffected by the specimen. Since the wave fronts of the two beams are coherent with respect to each other, they will interfere when superimposed. In a wide aperture (full-field) system, the resulting intensity distribution will yield an interferometric fringe pattern which is actually a contour map of constant optical path or optical phase difference.

Low frequency drift in the optical path, usually caused by such factors as temperature and pressure variations, vibrations of optical elements, and slow object motion, is a problem common to all vibration measuring interferometers. These low frequency effects reduce the effective sensitivity and/or range of the interferometer. Nevertheless, many investigators<sup>(1-10)</sup> have successfully demonstrated the use of interferometry as a tool for measuring the highly transient surface displacements associated with ultrasonic inspection procedures. To achieve the necessary sensitivity at high frequencies, these authors used either classical or holo interferometric arrangements. They have achieved adequate resolution but their systems use essentially laboratory/optical-bench types of devices that are not practical for adaptation to field applications. On the other hand, many fiber optic-based sensors have been designed to measure extremely small displacements encountered in quasi-static and low to intermediate frequency vibration studies.<sup>(11-16)</sup> While the resolution of these devices under ideal conditions is within the range required for ultrasonic testing, the combination of response time and sensitivity available with them were not, until now, high enough to permit the characterization of flaws by digital spectral analysis. In the present study it will be demonstrated that, by using high speed photoelectronics and fiber optic interferometry, this is no longer the case.

Limited access to the test specimen is another problem often encountered in applying interferometric measurements to ultrasonic inspection. Steering laser light with mirrors can be difficult when trying to interrogate even a small area of specimen surface in a confined space. The use of optical fibers to illuminate the test object and to sense the small surface displacements simplifies the problem of restricted access by guiding the beam to and from almost any spot on the specimen. The only limitation

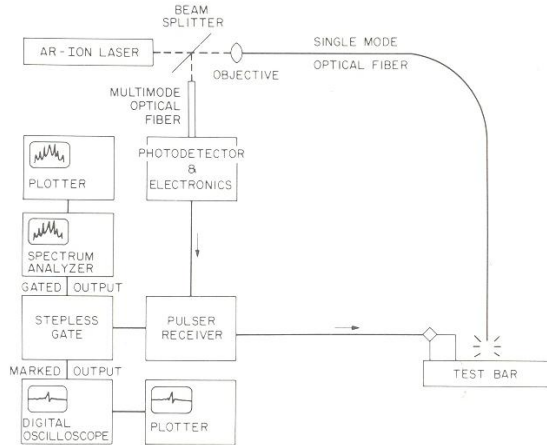


Fig. 1. Schematic of the test setup for the conventional *R*-wave excitation and OFI detection on a steel bar.

of optical fiber interferometry is that measurement is confined to sensing displacements at one "point" rather than full-field.

This paper describes the construction and operation of a single fiber optical fiber interferometer (OFI) capable of carrying out remote measurements of Rayleigh waves (surface acoustic waves, also called *R*-waves), sometimes in the presence of significant low-frequency ambient vibration. The design of this interferometer, shown in Fig. 1, is based on the Fizeau configuration. The unsplaid output from the laser is split by a variable beam splitter set to divide the output into two beams of equal intensity. One of the beams is wasted, the other is focused into a single mode optical fiber. This light travels down the optical fiber and a small percentage is internally (Fresnel) reflected at the output end. It then travels back through the fiber and serves as the reference wave. The remainder of the light emerges from the output end of the optical fiber and is scattered by the diffusely reflecting surface of the test subject. A small but detectable fraction of this scattered light is reflected back into the optical fiber to join and interfere with the internally reflected reference wave in its propagation back through the fiber. On exiting the optical fiber, the output is collimated by a focusing lens (the same lens used originally to launch the light into the fiber). The returning light is deflected by the beam splitter so that approximately half is passed through an aperture<sup>4</sup> onto one end of a multi-

<sup>4</sup>A collecting lens may also be of use with low intensity signals.

mode optical fiber whose opposite end is connected to a fast photodetector (photodiode with wide band amplification electronics). This multimode fiber is used to provide convenient coupling via its large (50  $\mu\text{m}$ ) core diameter. The phase preserving characteristic of a single mode optical fiber is not required because the phase related interference is established at the detection end of the single mode OFI fiber.<sup>5</sup> Therefore, only the amplitude (or intensity) of the returning light is significant.

Since the OFI is excited by coherent light, the two beams interfere destructively whenever the optical path lengths of the internally and externally reflected light beams differ by a half wavelength or odd multiple thereof. When the change in the displacement induced length of the Fizeau cavity is less than  $1/4$  wavelength the pure phase from OFI will define the displacement. If the intensities and polarizations of the internal and external reflections are reasonably equal, the intensity of the combined beams traveling back along the optical fiber will be seen to brighten and darken as the cavity length changes. A change in cavity length greater than  $1/4$  wavelength will shift the output signal intensity through one or more maxima and minima.

The intrinsic self-alignment of the reference and object beams is one important feature of the OFI. In addition, throughout most of the interferometer both beams experience the same environment—the relative phase of the two beams can change only in the Fizeau cavity. That is, the only place where the reference and object beams are not subject to the same temperature, pressure, vibration, etc. is in the cavity between the fiber tip and the specimen.

The only critical alignments of the entire system are those associated with launching the light into the fiber and separating out the returning signal. To receive the maximum signal from the OFI (when the Fresnel and the surface reflections are equal), a translation stage is used to move the fiber tip linearly in and out from the specimen surface. This permits the operator to adjust the amount of light recaptured by the fiber tip and thereby match the intensity of the internally reflected reference wave. If it were necessary to increase the intensity of the externally reflected return signal, as with a test surface of low reflectivity, a compact objective or rod lens could be added to the fiber tip to collimate the light as shown

by Kyuma *et al.*,<sup>(17)</sup> Hirose and Tsuzuki,<sup>(18)</sup> and Laming *et al.*<sup>(19)</sup> In the present tests on moderately reflective machined steel surfaces using an unlensed OFI, acceptable results were obtained with cavity lengths (or standoff distances) as long as 1 mm and as short as none.

Within the photodetector, the current generated by the photodiode was amplified, converted to a voltage and fed directly into an ultrasonic signal processing system incorporating a high pass filter amplifier and a stepless gate. This latter component was used to select desired parts of the time varying signal to be routed to an oscilloscope or spectrum analyzer for evaluation. Figure 1 shows the entire experimental set-up schematically, including both the optics and the electronics. Except for the OFI system (laser, optics, and fast photodetector), most of the instrumentation used in these experiments was the same as would be used in a typical experiment with wholly conventional ultrasonics.

### 3. ULTRASONIC EXPERIMENTS ON STEEL TEST BARS

The first tests were run using two standard piezoelectric transducers (with appropriate wedges) in the pitch-catch mode to generate and detect Rayleigh waves on the regularly machined (unpolished, flaw free) surface of a rectangular steel bar as shown in Fig. 2. Figures 3(a) and 3(b) show characteristic time and frequency domain plots of the Rayleigh wave responses obtained with a transducer

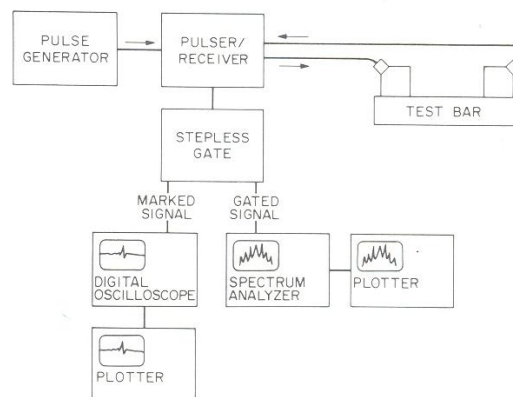


Fig. 2. Schematic of the test setup for a conventional *R*-wave pitch-catch interrogation of a steel bar.

<sup>5</sup>Actually, were it not for the high resolution required for the present experiments, multimode fiber could be used throughout the OFI.

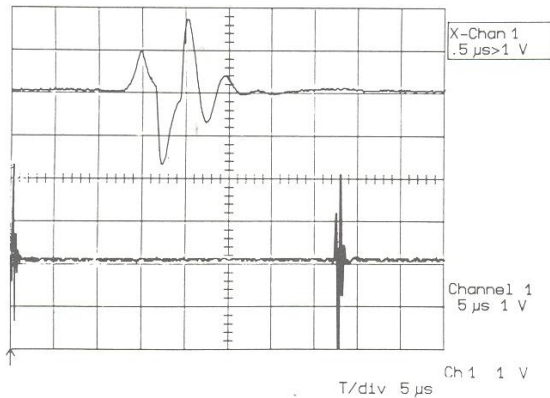


Fig. 3(a). Time domain (oscilloscope) plots of an *R*-wave generated by conventional pitch-catch on a flaw free steel bar obtained using piezoelectric transducers.

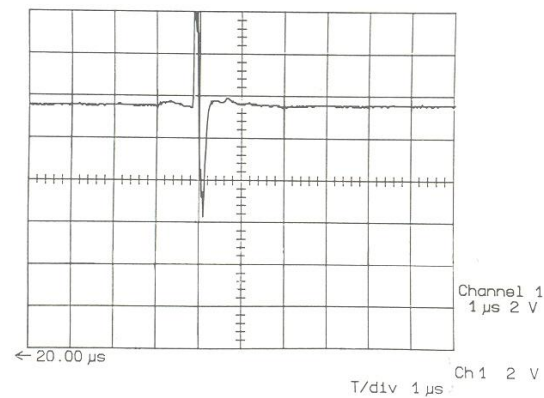


Fig. 4(a). Time domain (oscilloscope) gated output plot of an *R*-wave generated by a conventional transducer and detected by the OFI on the surface of a flaw free steel bar.

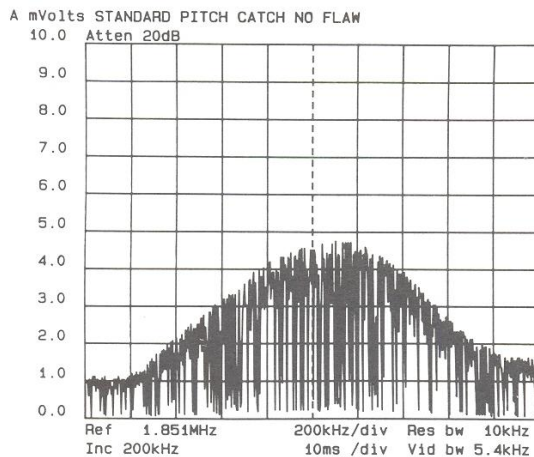


Fig. 3(b). Frequency domain (spectrum analyzer) plot of the *R*-wave shown in Fig. 3(a).

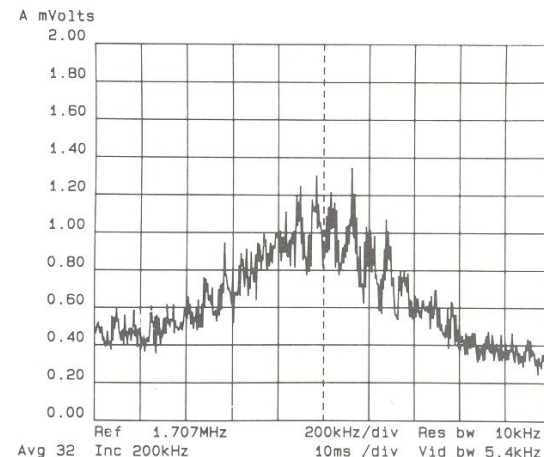


Fig. 4(b). Frequency domain (spectrum analyzer) gated output plot of the *R*-wave shown in Fig. 4(a).

wedge-face to wedge-face separation of 50 mm. With a Rayleigh wave velocity,  $C_R$ , in steel of 2.96 mm/ $\mu$ s, the travel time between transducers would be about 17  $\mu$ s. Since the time delay shown in Fig. 3(a) was around 37  $\mu$ s, the travel delay across the transducer wedges themselves must be around 20  $\mu$ s, or 10  $\mu$ s across each (since they are identical). When computing travel times in all subsequent experiments where the *R*-waves were generated using one of these trans-

ducer wedges and detected by the OFI, this 10  $\mu$ s interval delay must be subtracted from the measured times of flight. The upper trace in Fig. 3(a) shows a typical surface wave shape as detected by the piezoelectric transducer using an expanded time scale for the display. It can be seen from Fig. 3(b) that the center frequency of the transducers is a little over 2 MHz when in contact with the surface of the specimen.

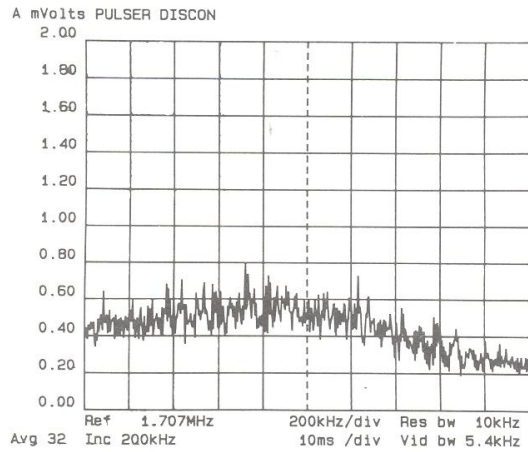


Fig. 4(c). Frequency domain (spectrum analyzer) noise spectrum of the OFI sensor (no excitation of steel bar).

Similar tests were run with the OFI used as a detector on a flaw-free surface in place of the piezoelectric transducer, and Figs. 4(a) and 4(b) show that comparable results were obtained. (Figure 4(c) shows the averaged noise in the frequency domain. It represents the frequency spectrum of the output for the time interval shown in Fig. 4(a), but with the cable between the pulser/receiver and the excitation transducer disconnected.) When a surface with a machined slit or "flaw" between the point of excitation and the OFI was tested with piezoelectric transducer excitation and OFI detection, the delay or "time-of-flight" of the *R*-wave was observed in the oscilloscope trace was seen to decrease as the OFI was moved towards the "flaw," exactly as expected. As the OFI was moved past the flaw, so that it was sensing at a point closer to the excitation than the flaw itself, Figs. 5(a) and 5(b), the main *R*-wave signal increased markedly in amplitude. Two additional signals also appeared as seen in Fig. 6(a). They are associated with components of the incident wave that was reflected from the two ends of the flaw. This figure is the time-domain record for a typical test with the transducers in the locations shown in Fig. 5b. The trace represents the ungated OFI signal transmitted to the oscilloscope through a high pass ( $> 1$  MHz) filter. The first peak,  $R_i$ , is the *R*-wave pulse generated by the piezoelectric transducer which was located 75 mm from the OFI. Adding the 10  $\mu$ s delay in the excitation transducer

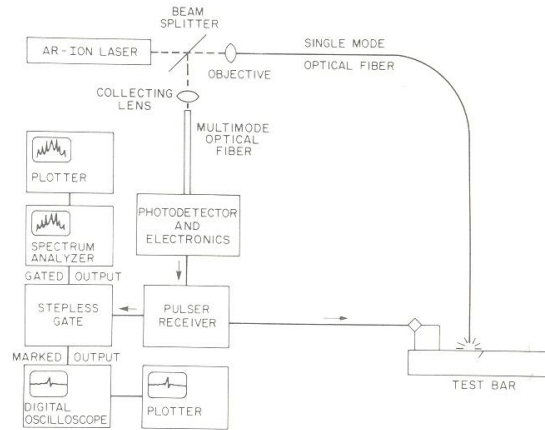


Fig. 5(a). Schematic of the test setup for the conventional *R*-wave excitation and OFI detection on a steel bar with a machined surface flaw.

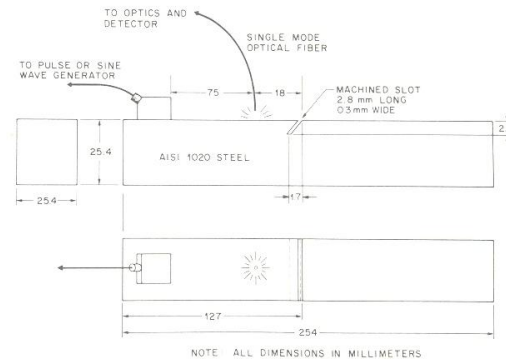


Fig. 5(b). Diagram of the geometry and instrumentation of the steel bar in Fig. 5(a).

wedge and using  $C_R = 2.96$  mm/ $\mu$ s predicts an *R*-wave travel time of 35  $\mu$ s—quite representative of the delay seen in the display. The next, strong peak represents the partially reflected wave,  $R_1$ , from the top of the machined surface flaw lying 18 mm beyond the OFI. This signal appears on the display almost 12  $\mu$ s after  $R_i$ , as it should. The second reflection,  $R_2$ , is from the bottom of the slot. The *R*-wave has traveled down and back up the 2.8 mm long slot. This additional 5.6  $\mu$ m travel distance accounts for the arrival of  $R_2$  about 2  $\mu$ s after  $R_1$ .

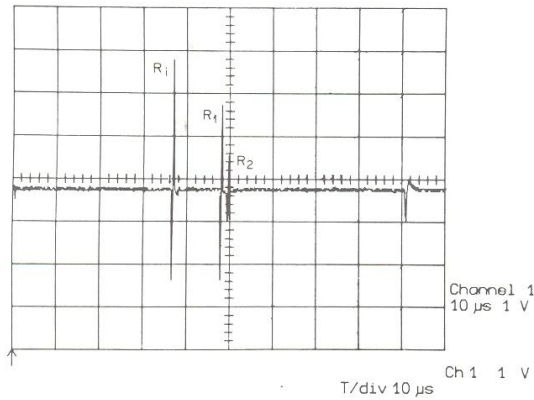


Fig. 6(a). Time domain (oscilloscope) plot of the input and reflected  $R$ -waves in a flawed steel bar obtained using the OFI sensor.

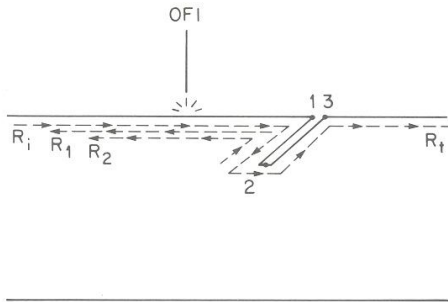


Fig. 6(b). Diagram showing the origins of the various  $R$ -waves detected by the OFI sensor.

The origins and paths of these waves are shown schematically in Fig. 6(b).

This clearly demonstrates two major advantages of the OFI over conventional piezoelectric transducers. First, because it does not involve the attachment of any energy absorbing mass to the surface at the point of measurement, OFI sensing does not itself in any way alter the acoustic wave. Consequently, the input and reflected waves may be monitored together. Second, the small sensing area of the OFI provides the high spatial resolution necessary for more accurate measurement of the time separation of closely spaced waves. This property is well illustrated by Fig. 6(a) where the clearly discernible

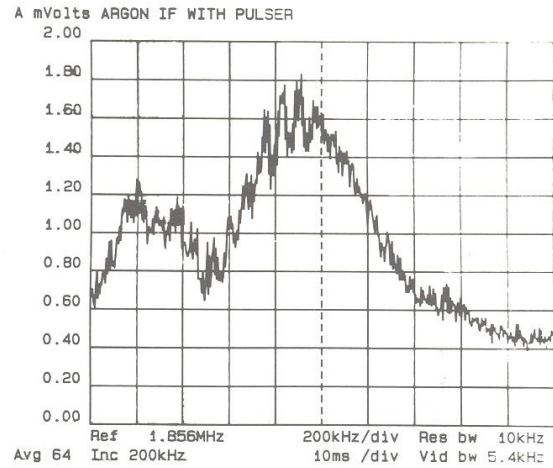


Fig. 7(a). Frequency domain (spectrum analyzer) plot of the input  $R$ -wave,  $R_i$ , in a flawed steel bar obtained using the OFI sensor.

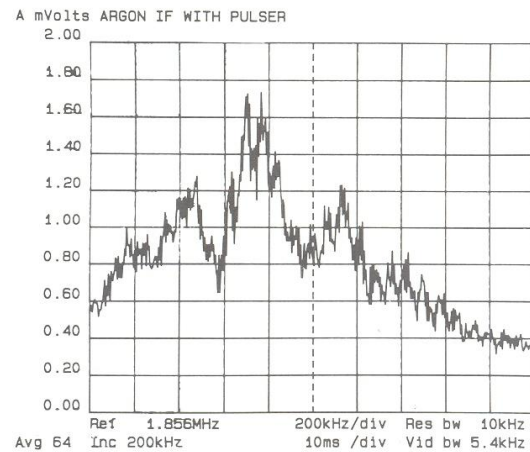


Fig. 7(b). Frequency domain (spectrum analyzer) plot of the reflected  $R$ -wave,  $R_1$ , in a flawed steel bar obtained using the OFI sensor.

arrival times of waves  $R_1$  and  $R_2$  may be used to estimate the length of a flaw.

Next a series of tests were run in which the OFI was used to monitor, successively, the response both in front of and behind the flaw in the test bar of Fig. 5. These signals were processed through the stepless

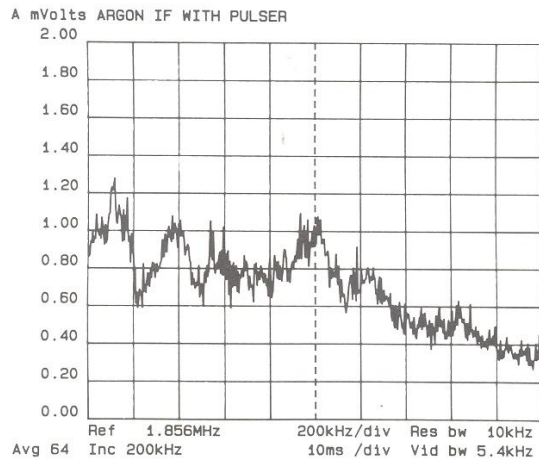
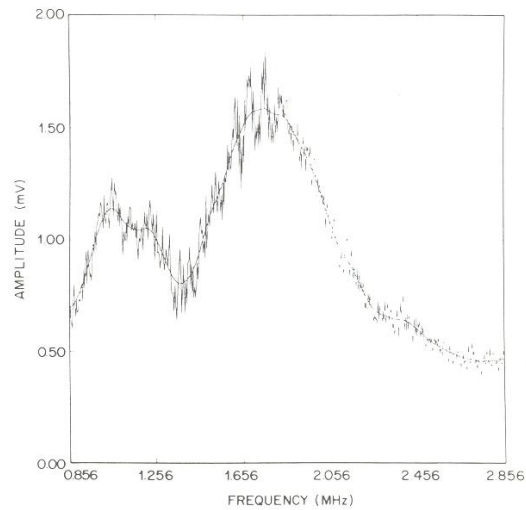


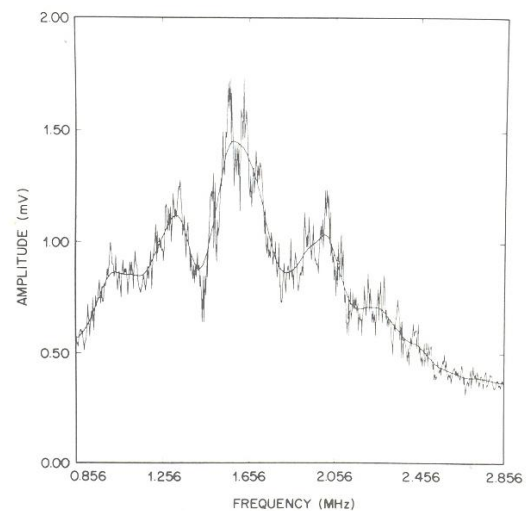
Fig. 7(c). Frequency domain (spectrum analyzer) plot of the transmitted  $R$ -wave,  $R_t$ , in a flawed steel bar obtained using the OFI sensor.

gate directly to the spectrum analyzer, instead of the oscilloscope, to yield frequency domain information. Figure 7(a) shows the spectrum of the input wave,  $R_i$ , and Fig. 7(b) shows the spectrum of the reflected wave obtained from the gated responses recorded with the OFI positioned 15 mm in front of the flaw, while Fig. 7(c) shows the spectrum of the transmitted wave obtained with the OFI positioned 15 mm beyond the flaw. The raw data sets from the analyzer were input into a computer where they could be smoothed by boxcar averaging across five frequency readings. Figures 8(a), 8(b) and 8(c) show the resulting smoothed curves obtained by repeating the boxcar averaging process twice to remove jitter, superimposed on the digitized data as plotted by the computer.

Finally, Figs. 9(a) and 9(b) show superpositions of the smoothed input, reflected and transmitted wave frequency data paired in various appropriate combinations. In Fig. 9(a), a superposition of the smoothed frequency data from the input and reflected waves, the curves show significant attenuation of the frequency components of the reflected wave centered around 1.8 MHz. There is additional attenuation around 2.15 MHz and in the frequency band between 1.0 and 1.15 MHz. The flaw depth of 2 mm corresponds to a frequency in steel of about 1.5 MHz. The incident wave has few components of lower frequency (longer wavelength). So, most of the



(a)



(b)

Fig. 8(a,b,c). Digitized and smoothed versions of the raw data in Figs. 7(a,b, and c), respectively.

frequencies in the incident wave are at least partially reflected by the flaw. However, components at frequencies that coincided with resonances of the free surface of the flaw are selectively attenuated. Three such points can be identified at 1.07, 1.81, and 2.15 MHz. The attenuation in the reflected wave spectrum at around 2.15 MHz ( $\lambda = 1.44$  mm) could be a second harmonic of the resonance at 1.07 MHz (2.8

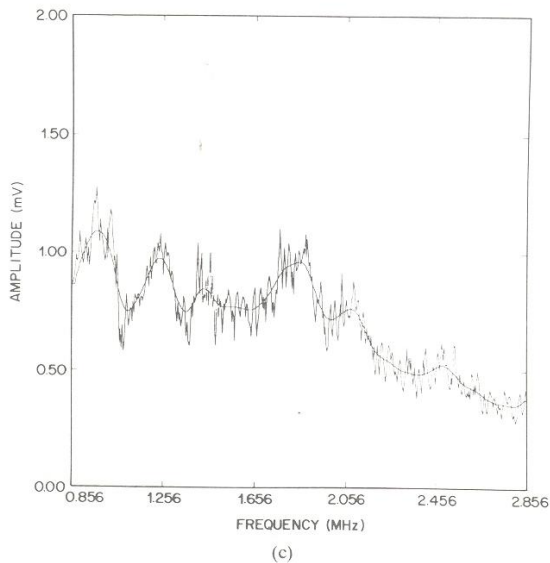
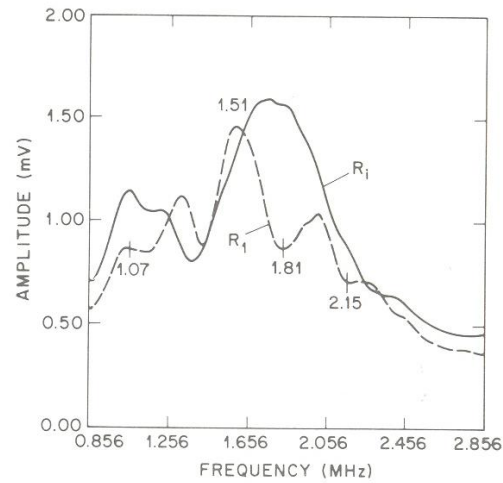
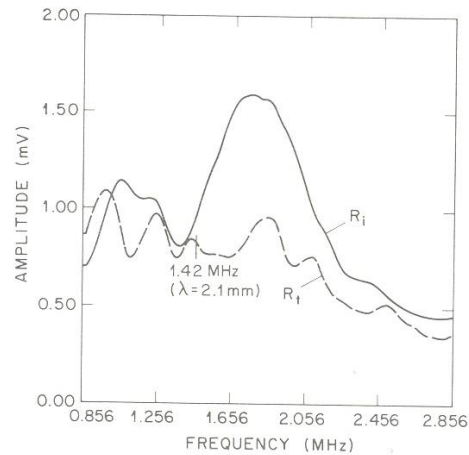


Fig. 8. Continued.

mm). It is interesting to note that a frequency of 1.07 MHz represents an acoustic wavelength of around 2.8 mm in steel. This coincides with the length of the flaw. The strong attenuation at 1.81 MHz relates to an elastic response that cannot readily be identified.

Figure 9(b) compares the spectrum of the input wave with that acquired by the OFI after transmission around and/or past the flaw. Here all frequencies above 1.42 MHz are significantly attenuated. Viktorov<sup>(20)</sup> shows that the out-of-plane amplitude of a Rayleigh wave attenuates rapidly with depth, and is less than 20% of its surface value at a depth of one acoustic wavelength. Since the flaw depth is 2 mm, components at frequencies higher than 1.4 MHz should be strongly represented in the reflected wave,  $R_r$ . Correspondingly the transmitted wave  $R_t$  would be deficient in frequencies higher than 1.5 MHz. Figure 9(b) confirms this. The lower frequency components, corresponding to acoustic wavelengths greater than the flaw depth, penetrate deeper than the flaw and should be well represented in  $R_t$ , as is the case. These results all suggest that the spectral differences between the input, reflected, and transmitted  $R$ -wave fronts as monitored by the OFI provide valuable information relating to the geometry of the surface flaw causing the reflection that could not readily be obtained using conventional piezoelectric transducer sensing.

Fig. 9(a). Plots of the smoothed frequency spectra of the input and reflected  $R$ -waves,  $R_i$  and  $R_r$ , in a flawed steel bar.Fig. 9(b). Plots of the smoothed frequency spectra of the input and transmitted  $R$ -waves,  $R_i$  and  $R_t$ , in a flawed steel bar.

#### 4. OFI SENSITIVITY

To make an estimate of the sensitivity of the OFI, a "calibration" experiment was run with the interferometer looking directly at the free surface of the piezoelectric crystal itself (no  $R$ -wedge, no steel bar test specimen) as shown in Fig. 10. In this

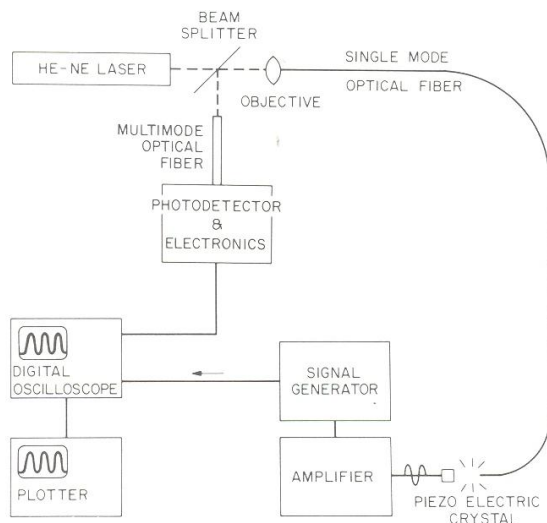


Fig. 10. Schematic of the test setup for the OFI sensor "calibration" experiment.

experiment the piezoelectric crystal transducer was driven by sinusoidal signals fed through a wide band amplifier at various frequencies, and both the input signals to the transducer and the OFI responses were monitored on the oscilloscope. According to the manufacturer of the piezoelectric transducer, 1 volt across the crystal produces  $0.4\text{\AA}$  ( $0.04\text{ nm}$ ) of normal surface displacement. The lower trace in Fig. 11 shows the  $\pm 4.25\text{V}$  input excitation that was supplied at 3 MHz to drive the transducer in the setup of Fig.

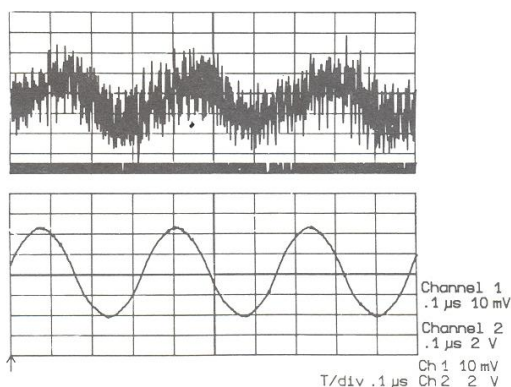


Fig. 11. Time domain (oscilloscope) plots of the sinusoidal crystal excitation (lower trace) and OFI sensor response (upper trace) at 3 MHz from the "calibration" experiment.

10. The top trace in Fig. 11 shows the signal obtained from the OFI sensor. If the  $0.4\text{\AA}/\text{V}$  responsivity has some relevance at 3 MHz (it is clear from Fig. 3(b) that there is no resonance at 3 MHz, so this is a reasonable assumption), this suggests that the OFI is following a vibration of around  $3.4\text{\AA}$  peak to peak. Unfortunately, because of the presence of ambient noise (both electronic and mechanical) and the limited accuracy of the available instrumentation, it was not possible to calibrate the OFI with greater precision. Clearly, the interferometer has extremely high resolution and bandwidth capabilities, but its operational sensitivity at acoustic wave frequencies remains to be determined.

## 5. OPTICAL FIBER INTERFEROMETER DEFICIENCIES AND LIMITATIONS

While the OFI shows great potential as a superior detector/sensor for ultrasonic NDE, its deficiencies and limitations should be noted. The primary alignment deficiency of the single fiber configuration used in this work arises from the difficulty sometimes encountered in separating the return signal from the input end reflection, which is quite strong. Fortunately, this problem can be solved by replacing the beam splitter and single optical fiber with a 3 dB bidirectional single mode optical fiber coupler<sup>6</sup> as shown in Fig. 12. This schematic also shows the use of a lens to concentrate the output, which, as mentioned earlier, can be a help in dealing with surfaces of poor reflectivity. If the bidirectional coupler is configured, as most are, with two forward outputs, it would be necessary to terminate the unused fiber in such a way as to minimize the internally reflected return signal. This could be done most simply by immersing the end of the fiber in an index matching fluid as shown in the schematic. At the other end, either of the optical fibers might be used for the laser input and the photodetector, since the device is actually a 3 dB or half power beam divider. Preferably, such a coupler should be highly stable, which can best be assured by using a fused coupler design. Subsequent reports will describe successful experi-

<sup>6</sup>Bidirectional couplers provide a means of dividing light from one fiber into two fibers, or combining light from two fibers into one, and usually involves an evanescent field coupling between the cores of two adjacent optical fibers. A useful discussion of single-mode bidirectional couplers may be found in the article by Tekippe and Wilson<sup>(22)</sup> published in the May 1985 issue of *Laser Focus*.

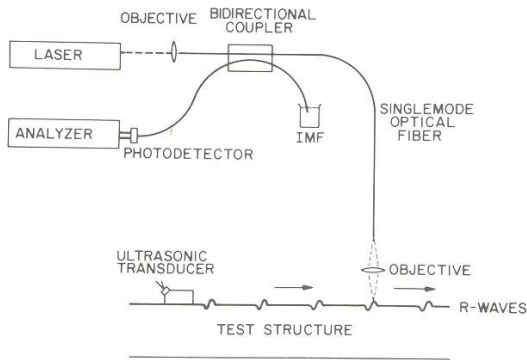


Fig. 12. Schematic showing the arrangement of a 3 dB bidirectional coupler used as a single point optical fiber interferometer for monitoring *R*-waves.

ments by the authors implementing such a bidirectional coupler based OFI for acoustic wave measurement.

There are also inherent limitations associated with the physics of an interferometer operated to yield high sensitivity and resolution at high frequencies. Since it is necessary to monitor displacements measured in the nanometer range at megahertz frequencies, it is to be expected that low frequency mechanical disturbances and high frequency electronic noise can create significant problems. All interferometers can be optimized by assuring maximum contrast—the greatest possible difference between the maximum and minimum intensities. Fortunately, for brightly reflecting surfaces this may be done simply by adjusting the stand-off (or cavity)

distance. However, with dark, poorly reflecting surfaces, scattering, polarization effects, and noise can be debilitating. (It should be noted, however, that in the “calibration” test described earlier, the signals shown were obtained from a vibrating black wear face that had only moderate reflectivity.) As in any half fringe interferometer used to achieve high resolution, maximum sensitivity and linear range are achieved with the cavity distance set to yield a signal mid-way between the highest and lowest intensities. At these extremes, which lie a quarter wavelength apart, the sensitivity falls to zero. Consequently, disturbances (such as thermal expansion, rigid body displacement, or low frequency mechanical vibration) which alter the relative spacing of the fiber tip and the test surface by a mere one eighth of an optical wavelength can shift the sensitivity from its maximum to nothing. Of course, low frequency ( $< 1$  MHz) vibrations of amplitudes significantly less than one eighth the optical wavelength can easily be filtered out of the signal electronically, but the larger amplitude disturbances must be carefully controlled lest they intermittently throw the OFI out of proper registration and temporarily destroy the signal. Note that one possible way of eliminating all long wavelength, low frequency mechanical noise of large amplitude (even several microns) would be to use both ends of a bidirectional coupler as a paired interference sensor to monitor relative surface motions at two points slightly more than one acoustic wavelength ( $\sim 3$  mm at 1 MHz in steel) apart as shown in Fig. 13. This would yield multiple signals, but since their relationship would be known, they would easily be interpreted accurately and the problem of mechanical noise

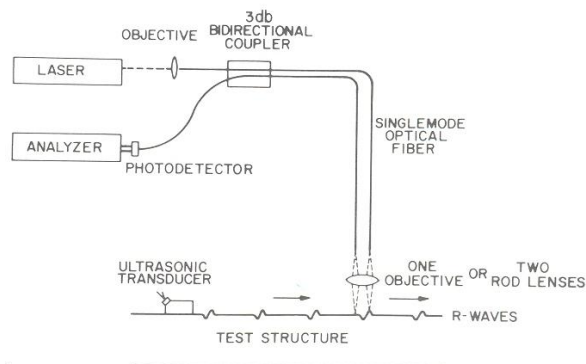


Fig. 13. Schematic showing the arrangement of a 3 dB bidirectional coupler used as a two point optical fiber interferometer for monitoring *R*-waves with minimum sensitivity to rigid body motions.

would be significantly reduced. The operation of such an OFI will be described in a subsequent report.

Finally, there is the matter of intermittent RF noise. Unfortunately, the high frequency electronics often act as an antenna and pick up signals in the MHz range that cannot be filtered without attenuating important components of the signal being studied. Such noise must be dealt with through good circuit design and component configuration, shielding, grounding, and so forth. In the present efforts, ad hoc coping was sometimes the only solution. This sometimes meant shutting down for a while until the noise went away (usually it was related to someone else's operation of a piece of poorly shielded equipment and/or unfortunate atmospheric conditions). On the whole, however, when the environment was reasonably quiet and the electronics in proper working order the OFI worked reliably and accurately.

## 6. CONCLUSIONS

Wide band OFI sensing has been shown to be a powerful tool of great potential for monitoring acoustic surface waves in steel, and likely many other important materials as well. Its point sensing and noncontact features permit the acquisition of considerably more information than can be obtained using a conventional piezoelectric transducer detector. Acousto-optic time-domain reflectometry has been shown to be an effective technique for the evaluation of OFI acoustic wave data. Such evaluation includes the identification of the presence, location, and possibly length of any isolated surface flaw whose dimensions lie within the measurable wavelength spectrum of the interrogating wavefront. It has also been shown that a properly gated spectrum analysis of OFI data may also be interpreted to provide information relating to the geometry of a surface flaw by comparing input, reflected, and transmitted *R*-wave spectra.

All these experiments have been concluded using pulsed piezoelectric *R*-wave transducers to generate surface waves appropriate to the detection and evaluation of surface flaws. However, earlier work by the present authors<sup>(21)</sup> has also shown that suitable acoustic waves may be generated by exciting a steel test bar with pulses of laser light guided through a noncontact optical fiber probe, and that such phonically generated acoustic waves may also be used to interrogate for flaws. The synthesis of these two

fiber optic-based techniques for the excitation, interrogation, and evaluation of materials and structures would provide a thermal-acousto-photonic (TAP) nondestructive evaluation capability with broad applications in many areas of reliability testing and certification. Moreover, whether used with conventional or fiber-optic based photo-acoustic wave excitation, OFI noncontacting sensors can readily be either (1) scanned across even complex surfaces or (2) configured in multiple sensor arrays to significantly enhance the interrogation and data gathering capabilities of TAP-NDE. Finally, since OFI sensors are flexible, compact, and readily engineerable into robust, steerable probes, they provide a potential means of inspecting many important structures that would not otherwise be accessible because of geometry, complexity, or scale.

## 7. ACKNOWLEDGMENTS

The authors wish to thank AT&T Bell Laboratories, Texas A&M University, the University of Alabama in Huntsville, and the U.S. Army Research Office under grant DAAL 03-86-K-0014 for their support of this effort. They also wish to express their thanks to R. O. Cook of Opto-Acoustic Sensors, Inc. for his many technical contributions. One of the authors (B. R. Peters) received a portion of his support from the American Society for Nondestructive Testing.

## REFERENCES

1. C. A. Calder and W. W. Wilcox, Noncontact material testing using laser energy deposition and interferometry, *Mat. Eval.* 86-91 (January 1980).
2. W. K. Lee and C. C. Davis, Laser interferometric studies of laser-induced surface heating and deformation, *IEEE, J. Quantum Electronics* QE-22(4): 569-573 (April 1986).
3. J. Monchalin, Optical detection of ultrasound at a distance by laser interferometry, *11th World Conf. on Nondes. Testing* (Am. Soc. of NDT, Columbus, Ohio, 1017-1024, 1985).
4. A. Aharoni and K. M. Jassby, Monitoring Surface Properties of Solids by Laser Based SAW Time-of-Flight Measurements, *IEEE Trans. on Ultrasonics Ferroelectrics and Frequency Control* UFFC-33(3): 250-256 (May 1986).
5. G. Birnbaum and G. S. White, Laser techniques in NDE, *Res. Tech. in NDT* (Academic Press, London, 1984) VII: 260-365.
6. C. H. Palmer, Optical probing of acoustic emission waves, *Proc. 23rd Conf. Non-Destructive Evaluation of Materials*, Raquette Lake, NY, August 1976 (Plenum Press, New York, NY, 1979) pp. 347-378.
7. R. E. Green, Jr., Some innovative techniques for nondestructive evaluation of materials, *Novel NDE Methods for Materials*

- (*Proc. Conf.*), Dallas, TX, 15–17 Feb. 1982 (The Metallurgical Society/AIME, 1983), pp. 131–139.
8. R. E. Green, Ultrasonic materials characterization, *Ultrasonics International 85* (Butterworth Scientific Ltd., 1985), pp. 11–16.
  9. C. A. Sciammarella, M. A. Asmadshani, and B. Subbaraman, Holographic interferometry measurement of ultrasonic vibration amplitudes, *Proc. 1986 Spring Meeting* (Soc. for Exp. Mech., New Orleans, Louisiana, June 1986), pp. 706–710.
  10. B. B. Djordjevic and R. E. Green, High speed capture of acoustic emission and ultrasonic transients as detected with optical laser beam probes, *Proc. of the Ultrasonic International Conference* (Grav, Austria, 1979), pp. 82–87.
  11. R. O. Cook, and C. W. Hamm, Fiber optic lever displacement transducer, *Appl. Optics* **18**(19): 3230–3241 (October 1979).
  12. B. Culshaw, Fiber optic sensing techniques, *Res. Rech. in NDT* (Academic Press, London, 1984), VII: 191–215.
  13. B. J. Hogan, Fiber-optic interferometer measures  $10^{-9}$  cm displacement, *Design News* **3**(1): 62–63 (1972).
  14. J. C. Wade, P. S. Zerwekh, and R. O. Claus, Detection of acoustic emission in composites by optical fiber interferometry, *Proc. of the 1981 IEEE Ultrasonics Symposium* (Chicago, Illinois, October 1981).
  15. S. Ueha, N. Shibata, and J. Tsujiuchi, Flexible coherent optical probe for vibrational measurements, *Optical Commun.* **23**(3): 407–409 (1977).
  16. A. D. Drake and D. C. Leiner, Fiber-optic interferometer for remote subangstrom vibration measurement, *Rev. Sci. Instrum.* **55**(2): 162–165 (February 1984).
  17. K. Kyuma, S. Tai, K. Hamanaka, and M. Numosuto, Laser doppler velocimeter with a novel optical fiber probe, *Appl. Optics* **20**(14): 2424–2427 (1981).
  18. Y. Hirose and Y. Tsuzuki, Optical fiber sensing for three dimensional vibration measurements, *Proc. 2nd Int'l. Conf. on Optical Fiber Sensors*, (NTG, Stuttgart, 1984), pp. 415–478.
  19. R. I. Laming, M. P. Gold, D. N. Payne, and N. A. Halliwell, Fiber-optic vibration probe, *SPIE, Fiber Optic Sensors* **586**: 38–44 (1985).
  20. I. A. Viktorov, *Rayleigh and Lamb Waves* (Plenum Press, New York, 1967).
  21. G. P. Burger, T. D. Dudderar, J. A. Gilbert, B. R. Peters, and J. A. Smith, Laser excitation through fiber optics for NDE, *J. Nondestruct. Eval.* **6**: 57–64 (1987).
  22. V. J. Tekippe and W. R. Wilson, Single-mode directional couplers, *Laser Focus* **21**(S): 132–144 (1985).